Flutter of Orthotropic Panels at Arbitrary Yaw Angles— Experiment and Theory

Peter Shyprykevich*

Grumman Aerospace Corporation, Bethpage, N.Y.

and

James Wayne Sawyer‡

NASA Langley Research Center, Hampton, Va.

Experimental flutter boundaries were obtained for yaw angles between 15° and 90° at Mach numbers 2 and 1.6 for panels mounted on a remotely controlled turntable. Good definition of the flutter boundaries was obtained by rotating the panels into and out of flutter. Two types of specimens were tested: a single sheet corrugated panel having a length-to-width ratio of 5 on clamped supports; and several square doubly-corrugated panels on various flexible supports. Calculated flutter speeds based on quasi-steady aerodynamics are compared to experimental data.

Nomenclature

a	= panel length (x-direction)
b	= panel width (y-direction)
D_1	= $D_x/(1 - \mu_x \mu_y)$
D_2	= $D_y/(1 - \mu_x \mu_y)$
D_{12}	= $D_{xy} + \mu_x D_2$
D_x, D_y	= panel bending stiffnesses in x- and y-directions, respectively
D_{xy}	= panel twisting stiffness
f	= frequency
f_{cr}	= flutter frequency
K_D, K_R, K_T	= deflectional, rotational, and torsional spring constants, respectively, per unit length
$\bar{K}_D$	= $(K_D/D_1)(a/\pi)^3$, nondimensional deflectional spring constant
$\bar{K}_R$	= $K_R a/D_1 \pi$, nondimensional rotational spring constant
$\bar{K}_T$	= $K_T a/D_1 \pi$, nondimensional torsional spring constant
M	= Mach number
m, n	= number of half-waves in x, y directions, respectively
q	= dynamic pressure of airstream
q_{cr}	= dynamic pressure of airstream at flutter
x, y	= Cartesian coordinates of panel
β	= $(M^2 - 1)^{1/2}$
Λ	= yaw angle
λ	= dynamic pressure parameter, $2qa^3/D_1 \beta$
λ_{cr}	= dynamic pressure parameter at flutter
μ_x, μ_y	= Poisson's ratio associated with curvature in y- and x-directions, respectively

Introduction

A CANDIDATE for the thermal protection system of high speed re-entry and hypersonic vehicles is the corrugated metallic panel constructed of high temperature alloy. Such a panel may be idealized as an orthotropic plate with either flexible or rigid supports. Flexible supports are often necessary to accommodate thermal expansion without creating large thermal stresses. Ideally, such a panel would be aligned on the vehicle with the corruga-
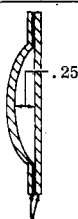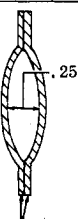
tions parallel to the air flow. However, in a typical flight trajectory, various degrees of cross flow will be encountered, which, according to analysis, may reduce flutter margins drastically.[1] Since available wind tunnel data were insufficient to substantiate these analytical predictions, a test program was conducted to provide such data. Specifically, various types of orthotropic panels were designed, analyzed, and fabricated, and were tested in the Unitary Plan Wind Tunnel at the NASA Langley Research Center. The results of this test program and the comparison with theory are the basis of this paper.

Test Apparatus

Panels

The test panels (aluminum) were designed to simulate various stiffness parameters and support conditions. The summary of panel types is given in Table 1. The single corrugation panel is representative of the torsionally weak construction, and the doubly corrugated panel of the torsionally strong construction. The single corrugated panel was formed from a 0.010 in. sheet, and was bolted directly to a ½ in. thick aluminum supporting plate as shown in Fig. 1. The bolt spacing was 1 in. The doubly-corrugated panels were formed from 0.008 in. sheets, and

Table 1　Panel types

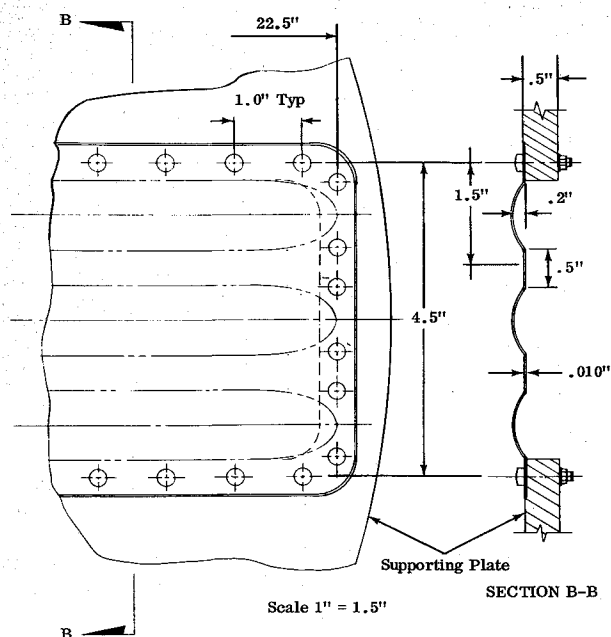|	Corrugation		
	Single	Double	Double
Cross-Section	.2" .010"	.25" .008"	.25" .008"
a(in.)	22.5	14.0	14.0
a/b	5.0	0.935	0.935
D_2(lb-in.)	0.88	3.58	3.58
D_1/D_2	755	420	270
D_{12}/D_2	1.5	137	146

Fig. 1 Single corrugation panel.

joined by spot welding along their lengths at the flat part between corrugations. Except for the different cross-sections, the doubly corrugated panels were identical in construction and were similarly supported. These panels were bolted directly to the circular supporting plate on two opposite sides and mounted on discrete clips on the other two sides as shown in Fig. 2. The clips were attached to the supporting plate with either the inner and the two outer screws or with just the two outer screws. This provided two different support stiffnesses. Since the clips were manufactured in two thicknesses (0.024 in. and 0.018 in.), several flutter models were available when these were combined with the panels. The panel with the flat sheet was tested twice, once with the flat side exposed to the flow and the second time with the corrugations exposed to the flow in order to evaluate the effect of beading on panel flutter.

As shown previously, the test panels were mounted on a circular plate which subsequently was attached to a turntable. For the doubly corrugated panels, additional fairings were provided to smooth the air flow over the panel. No fairings were needed for the single corrugation panel since the beads were closed out. The turntable itself was mounted vertically in a splitter plate which was projected into the airstream from the tunnel sidewall so that the
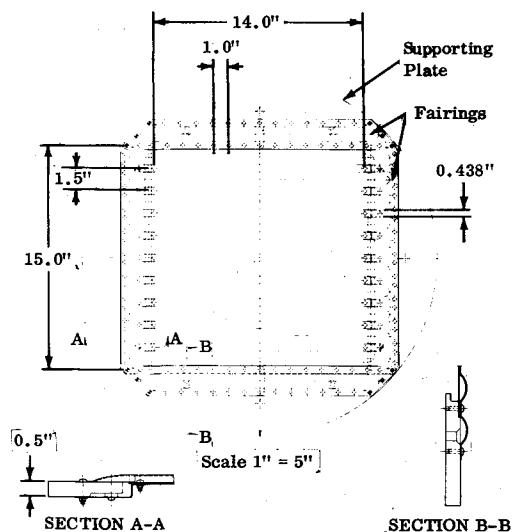
tests were conducted free of the tunnel boundary layer. The whole arrangement is shown in Fig. 3. The cavity pressure behind the panel was controlled manually by a 1 in. diam line attached to a vacuum pump.

Instrumentation

Each panel specimen was instrumented with eight strain gages and five thermocouples. Signals from the strain gages were used during testing to detect the onset of flutter and to measure flutter frequency. The thermocouples were monitored during test to assure that temperature differential on the panel was a minimum during the measurement of the flutter threshold. Yaw angles were measured visually through the tunnel window.

In addition to panel instrumentation, a calibration plate (similar to panel supporting plates) with 11 pressure taps was installed in the turntable to measure the pressure variation over the turntable area where the panel models were to be located. Seven pressure taps were located along the centerline of the turntable in the direction of the flow. Pressures were recorded on a scanivalve for $M = 2$ and $M = 1.6$ and for the wind-tunnel range of dynamic pressures.

Wind Tunnel

Flutter tests were conducted in the Langley Unitary Plan wind tunnel at Mach numbers of 2 and 1.6. The dynamic pressure in that tunnel is continuously variable. The maximum levels attained at Mach numbers 2 and 1.6 were 1779 psf and 1475 psf, respectively. The freestream stagnation temperature varied between 100° and 130°F.

Test Procedure

Vibration and Static Tests

Vibration surveys and static tests were performed to check panel and support stiffnesses. For the vibration surveys, the panels were mounted in the circular supporting plate and excited by one or two air shakers. Node lines were determined using a deflectometer mounted on a movable arm. These tests were conducted without simulating the effect of the cavity. Once the panels were in the turntable on the splitter plate, the shake tests were repeated at ambient pressure with the actual sealed cavity. No appreciable change in frequencies was observed. Clip flexibilities were also checked statically by loading the clip with forces and moments and measuring the resulting displacements and rotations.
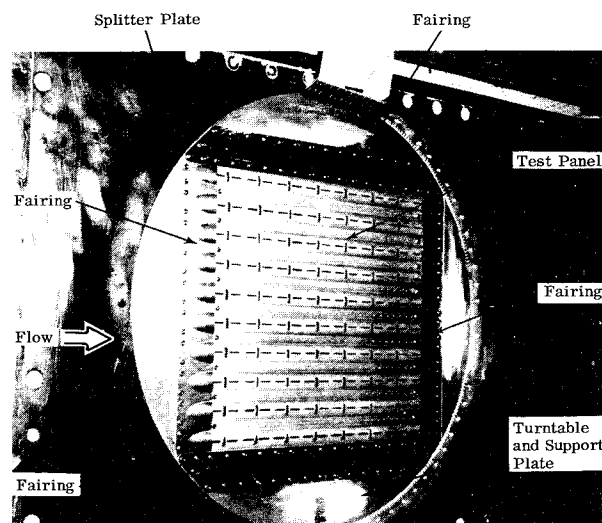

Fig. 2 Double corrugation panel.

Fig. 3 Doubly corrugated panel mounted in the splitter plate.

Flutter Tests

Before the test models were inserted into the airstream, the calibration plate with the pressure taps was installed in the turntable. Steady-state pressure distributions were measured over the turntable area where panel models were to be located. These pressures were used to determine pressure loading on the panels, and the cavity pressure setting which would result in zero differential loading. Relatively low pressure variations were obtained over the panel at $M = 2$ at low and intermediate dynamic pressures. However, large pressure variations existed at $M = 1.6$ and at $M = 2$ at high dynamic pressure levels.

The usual test procedure consisted of establishing constant temperature, dynamic pressure, and Mach number, and then rotating the panel away from zero yaw angle until flutter was initiated. During this time, cavity pressure was manipulated to maintain zero pressure loading on the panel. At a particular dynamic pressure, a flutter point was defined as the lowest angle at which flutter could be induced with zero pressure loading on the panel. Once the flutter point was reached, the panel was rotated back to a smaller yaw angle and the dynamic pressure increased by a certain increment. This procedure was con-

Fig. 4 Strain gage response during flutter.

tinued until the maximum wind-tunnel dynamic pressure was attained. In this way the flutter boundary as a function of yaw angle was obtained. Since the turntable was power-driven, quick excursions into and out of flutter were possible. A typical trace of a strain gage response before and after initiation of flutter is shown in Fig. 4.

Table 2 Panel flutter models

Panel No.	Type	a (in)	$\frac{a}{b}$	D_2(lb-in)	$\frac{D_1}{D_2}$	$\frac{D_{12}}{D_2}$	Support Along y-Edges*	Calculated Support Stiffnesses	Support Stiffnesses for "Best Fit"
1	Single Corrugation	22.5	5.0	0.88	755	1.5	clamped	$\bar{K}_D = \infty$ $\bar{K}_R = \infty$	Not Applicable
2	Double corrugation: Flat sheet joined with corruga-tion sheet. Flat sheet exposed to airflow.	14.0	0.933	3.58	420	137	.024" clips with 3 screws	$\bar{K}_D = 1.12$ $\bar{K}_R = .022$ $\bar{K}_T = .016$	$\bar{K}_D = 1.12$ $\bar{K}_R = 1.9$ $\bar{K}_T = .12$
3	Double corrugation: Flat sheet joined with corrugated sheet. Corrugated sheet exposed to airflow.	14.0	0.933	3.58	420	137	.024" clips with 3 screws	$\bar{K}_D = 1.12$ $\bar{K}_R = .022$ $\bar{K}_T = .016$	$\bar{K}_D = 1.12$ $\bar{K}_R = .022$ $\bar{K}_T = .30$
4	Double corrugation: Flat sheet joined with corrugated sheet. Flat sheet exposed to airflow.	14.0	0.933	3.58	420	137	.024" clips with 2 screws	$\bar{K}_D = .245$ $\bar{K}_R = .013$ $\bar{K}_T = .008$	$\bar{K}_D = .245$ $\bar{K}_R = .013$ $\bar{K}_T = .008$
5	Double corrugation. Two joined corrugated sheets.	14.0	0.933	3.58	270	146	.018" clips with 3 screws	$\bar{K}_D = .692$ $\bar{K}_R = .014$ $\bar{K}_T = .007$	$\bar{K}_D = .692$ $\bar{K}_R = .014$ $\bar{K}_T = .30$

*Except for panel 1, x-edges are assumed to be simply supported.

Table 3 Panel natural frequencies

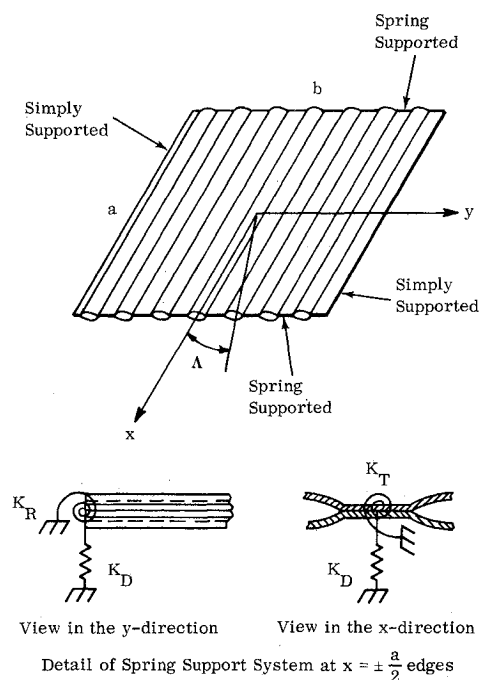| Panel No.	n m	Measured, Hz 1	2	3	4	Calculated, Hz 1	2	3	4	Calculated "Best Fit", Hz 1	2	3	4
1	1	152	347	696		150	296	545					
	2	270				328				Not applicable.			
	3	523				618							
2	1	120	136	166	255	104	117	134	162	115	137	165	205
	2					222							
	3												
3	1	116	160	200	285	104	117	134	162	111	147	196	254
	2	310				222				261			
	3												
4	1	58	73	85	110	56	64	84	120	56	64	84	120
	2												
	3												
5	1		124	165	202	71	79	96	127	80	114	158	211
	2												
	3												

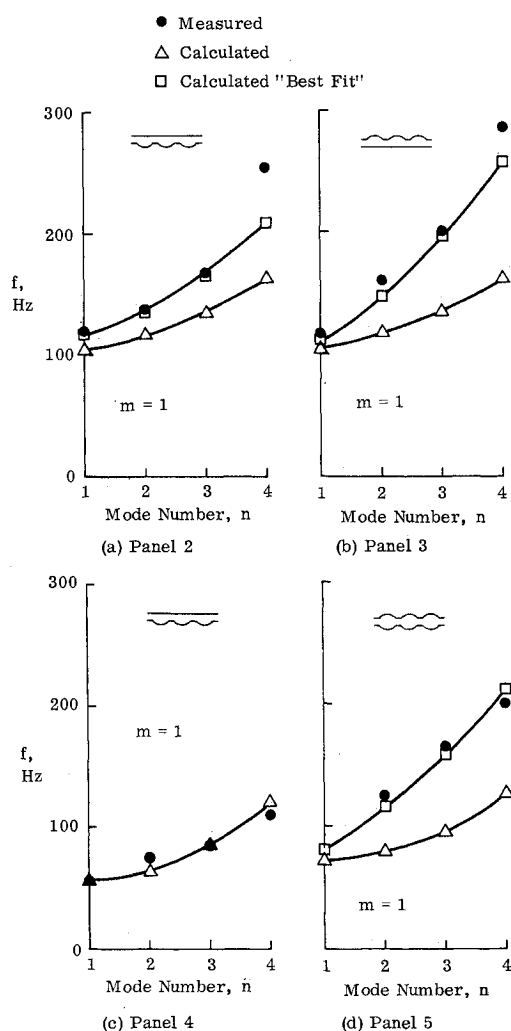Fig. 5 Schematic of orthotropic panel and support system.

Fig. 6 Comparison of experimental and theoretical natural frequencies.

High speed 16 mm movies were taken for two panels. They confirm the theoretical predictions[3] that the flutter motion is concentrated towards the trailing edge of the panel.
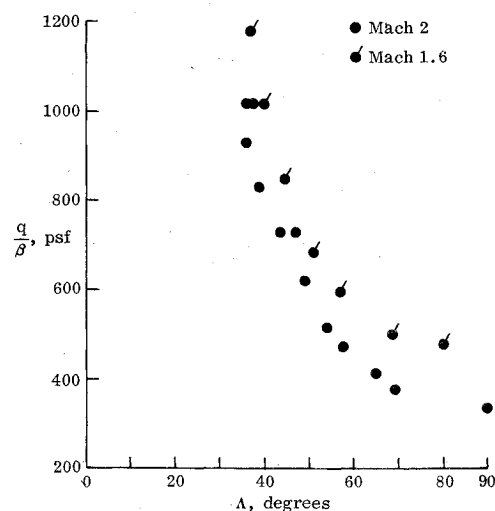

Fig. 7 Comparison of experimental flutter boundaries at $M = 2$ and $M = 1.6$ for Panel 3.
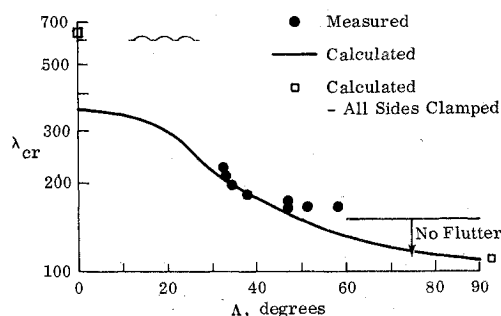

Fig. 8 Comparison of experimental and theoretical flutter boundaries for Panel 1 at $M = 2.0$.

Results and Discussion

Experimental and Analytical Frequency Comparisons

The combinations of panels and support stiffnesses studied are listed in Table 2, and the corresponding measured and calculated frequencies are given in Table 3. The coordinate system and the various panel and support parameters are defined in Fig. 5. Panel stiffness properties were computed using the method of Stroud,[2] and clip stiffness properties were calculated using strain energy methods. Natural frequencies were then obtained using a Galerkin-type solution.[3]

Reasonably good correlation between experimental and analytical frequencies was obtained for panel 1. This panel is effectively square, since the greater bending stiffness in the x direction is counterbalanced by the longer span. In the short direction, the measured frequencies are somewhat higher than the calculated values, and in the long direction the opposite is true. The discrepancies are attributed to the not fully clamped condition of the short edges and curvature effects. However, no attempts were made to vary the theoretical panel bending properties to account for the differences.

For panels 2-5, the initial comparison of frequencies between test and analysis was poor. Since the measured individual clip deflectional spring constant compared very well with the calculated value, the more doubtful values of rotational and torsional spring constants were changed to improve correlation. Clip stiffness properties corresponding to the "best fit" with the measured frequencies are listed in the last column of Table 2, and the resulting frequencies in the last four columns of Table 3.

The improvement in frequency correlation is shown graphically in Fig. 6, where the calculated frequencies for
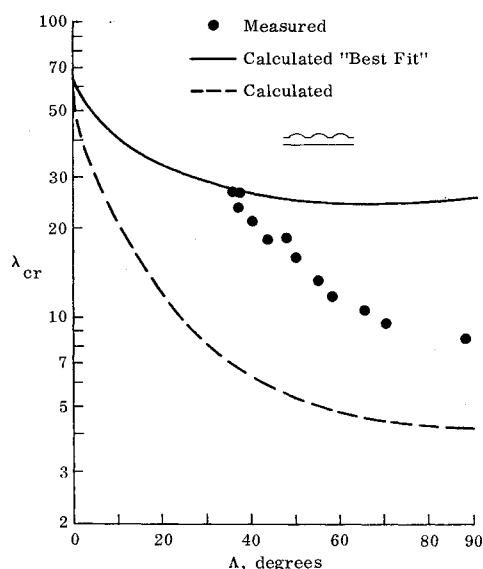
Fig. 9 Comparison of experimental and theoretical flutter boundaries for Panel 2 at $M = 2.0$.
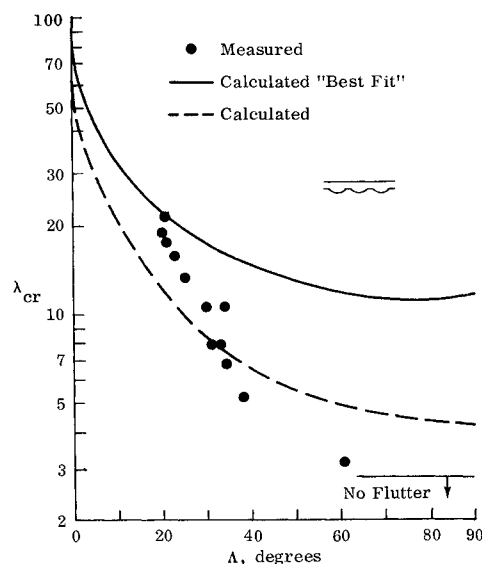

Fig. 10 Comparison of experimental and theoretical flutter boundaries for Panel 3 at $M = 2.0$.

the initial and "best fit" support stiffnesses and the measured frequencies are plotted against weak direction mode numbers. The torsional spring constant K_T was found to be the only effective parameter influencing higher modes. The rotational spring constant K_R influenced only low modal frequencies.

As seen in Fig. 6c, the initial calculated frequencies for panel 4 (clips attached to the panel only by two outer screws) compared reasonably to measured frequencies. This reinforced the assumption that the calculated panel stiffnesses were correct, and that for clips attached by three screws, frequency discrepancies were due to the underestimation of support stiffnesses.

Panels 2 and 3 were identical except that different sides were exposed to the flow. One would expect identical frequency responses. However, the vibration tests have indicated consistently different behavior, especially for second and higher modes. This is attributed to panel warping and to attachment differences, and is reflected in the different "best fit" stiffness values of supports. There is a shift in the location of the panel neutral axis in relation to the clip attachment. This explains, at least partially, the different "best fit" K_R values. To put the correlation for panels 2–5 into perspective, it is noted that similar results for corrugated panels have been obtained previously by other investigators.[4]

Experimental Flutter Results

Flutter boundaries as a function of yaw angle for all panels listed in Table 2 are presented in Fig. 7–12. Because of wind tunnel dynamic pressure limitations, no flutter points were reached between 0° and 15°, and in most cases flutter was obtained only between 30° and 90°. An unusually small amount of data scatter was encountered. This is attributed to: 1) the ease of initiating and stopping flutter by rotating the turntable; and, 2) the small temperature effects due to the type of panel design.

Some of the difficulties encountered during testing were with the cavity pressure control and pressure variations over the panels. At $M = 1.6$, and at $M = 2$ at low dynamic pressures, leakage around the turntable was too high to permit satisfactory manual control of the cavity pressure. For this reason, the normalized flutter dynamic pressures (q/β) shown in Fig. 7 are higher at $M = 1.6$ than at $M = 2$, despite the fact that Lemley[5] suggests that the $M = 1.6$ boundary should be below the $M = 2$ curve. Also, due to higher pressure variations over the panels at high dynamic

pressures, experimental flutter trends at low yaw angles were more difficult to define. This was especially true for panel 4, which had the lowest support stiffness (see Fig. 11).

Except for panel 3, flutter frequencies were measured concurrently with the flutter dynamic pressures. They are plotted as a function of yaw angle in Fig. 13. The scatter in flutter frequencies is of the same order as that for the flutter dynamic pressures, with the maximum deviation again occurring for panel 4. Considering all of the above factors, the $M = 2$ results were judged superior to the $M = 1.6$ results, and accordingly the former were used for correlation with theory.

Correlation with Theory

The flutter analysis used for comparison with the experimental data is a generalization to account for flow angularity of the procedure due to Heard and Bohon.[3] This is a Galerkin-type solution for an orthotropic panel on continuous deflectional, rotational, and torsional springs along two opposite edges, and simply supported along the other two sides. Pressure loading is obtained using static piston-
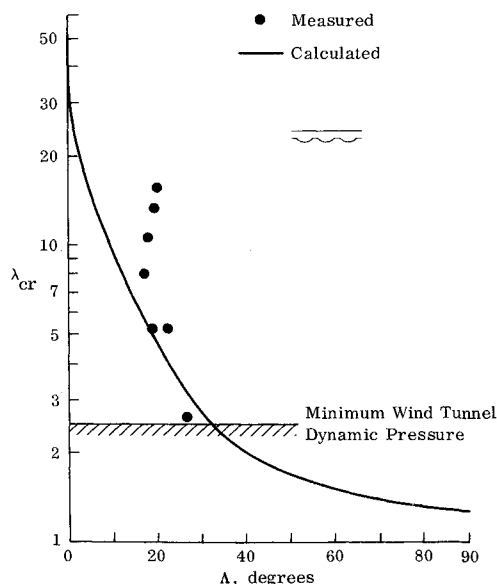

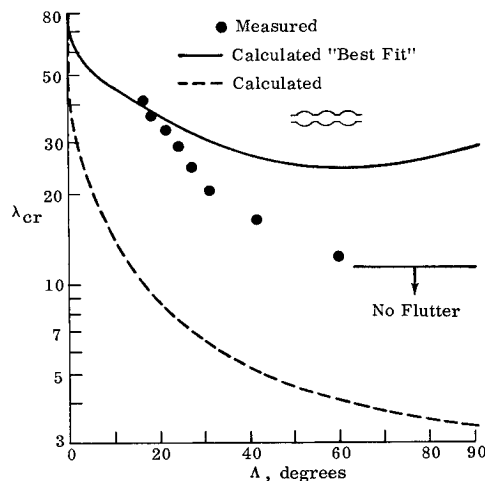Fig. 11 Comparison of experimental and theoretical flutter boundaries for Panel 4 at $M = 2.0$.

Fig. 12 Comparison of experimental and theoretical flutter boundaries for Panel 5 at $M = 2.0$.

theory aerodynamics. Flutter is defined as the lowest dynamic pressure corresponding to a coalescence of any two modes. Numerical results presented here represent converged values using as many as thirty modes.

At this point, it should be emphasized that the above analysis requires two opposite sides of the panel to be simply supported, whereas, for the test panels these sides were essentially clamped. For the square panels (panels 2–5), this approximation is certainly valid, since the effective length of the panel in the y direction is extremely large, and the $y = \pm b/2$ edges do not influence either the panel natural frequencies or panel flutter dynamic pressures. For panel 1, which has four clamped sides, it was found that the best flutter results, at least for the range of yaw angle where test data was available, were obtained by making the short rather than the long sides simply supported. These results are presented in Fig. 8, where in addition, flutter points at $\Lambda = 0°$ and $90°$ for a clamped-clamped analysis[6] are shown. At $\Lambda = 90°$, the λ_{cr} is the same whether the y-edges are simply supported or clamped.

For panel 4, for which initially good frequency correlation was obtained, good flutter comparisons between test and analysis are also evident (Fig. 11) for the very limited range of yaw angle. The deviation of test values at lower angles can be attributed, as stated previously, to the build-up of pressure loading at these dynamic pressure levels.

For all other panels, correlation is not as good. The discrete flexible supports introduce an additional set of variables having a large influence on flutter. Calculated flutter speeds at high yaw angles are particularly sensitive to the torsional stiffness of the supports. This is illustrated in Fig. 10, where the calculated flutter parameter λ_{cr} is plotted for $\bar{K}_T = 0.016$ and $\bar{K}_T = 0.30$. $\bar{K}_T = 0.016$ is the value for one clip calculated using strain energy methods and dividing the value by clip spacing. $\bar{K}_T = 0.30$ represents the "best fit" value based on test natural frequencies. The λ_{cr} at $\Lambda = 90°$ is six times greater for $\bar{K}_T = 0.30$ than for $\bar{K}_T = 0.016$. Because of this wide range of possible calculated values, it was felt that a more realistic approach to correlation would be to present both of the calculated flutter boundaries with the test results. Thus for panels 2, 3, and 5, two analytical flutter boundaries and one experimental boundary are given in Figs. 9, 10, and 12, respectively.

Test results for panels 3 and 5, in Figs. 10 and 12, fall between the two analytical flutter points at $\Lambda = 90°$ and approach the upper boundary at lower yaw angles. Corre-

lation improves in the yaw angle region where the effect of torsional spring supports is smaller. Repeatability of test results is very evident for these two similar panels. It should be noted that for both panels corrugations are exposed to the flow.

The configuration of panel 2 is identical to panel 3 except that the flat sheet is exposed to the air flow. The test flutter boundary (Fig. 9) is, however, quite different. λ_{cr} values for panel 2 are less than one third of those for panel 3. Some of the difference can be explained by the different "best fit" stiffness characteristics as shown in Table 2. However, it should be noted that panel 2 is the only one for which the test flutter boundary falls below the lower analytical boundary. This implies that exposing the beaded surface to the flow is beneficial for panel flutter.

A possible reason for the "best fit" flutter boundaries falling above the test data for large yaw angles is the overestimation of D_{12} for the doubly corrugated panels. Stroud[2] indicates that the correlation of the calculated D_{12} with test values is highly dependent on the type of cross section. Furthermore, cross sections of the test panels in this investigation are open at the ends and accordingly their full torsional stiffness is not developed until some distance from the supports.

Conclusions

Flutter characteristics of two types of corrugation-stiffened panels at various yaw angles were studied both experimentally and analytically. Flutter tests were made at Mach numbers 2 and 1.6. Analyses were based on quasi-steady aerodynamics and neglect panel beading. In addition, vibration tests and analyses were performed.

The experimental part of the study has shown that repeatable flutter boundaries can be obtained if care is taken in eliminating thermal stresses in panel models. A unique feature of this study was the use of a remotely controlled turntable to rotate test panels. Rotating the test panel to initiate and stop flutter clearly delineated the onset of flutter.

For moderate yaw angles, when a large component of the flow is along the corrugations, correlation with theory was good, but as the flow became perpendicular to the corrugations, large discrepancies between test and theory are apparent. Since for this configuration flutter is extremely sensitive to boundary conditions, a better definition of the structure is needed.

It can also be concluded that beaded surfaces have a stabilizing effect on flutter, though their exact influence is difficult to determine because of the large effect of other parameters.

References

[1]Bohon, H. L. and Shore, C. P., "Application of Recent Panel Flutter Research to the Space Shuttle—Part II, Influence of Edge Clips and Flow Angularity," TM X-2274, Vol. III, April 1971, NASA.

[2]Stroud, W. J., "Elastic Constants for Bending and Twisting of Corrugation-Stiffened Panels," TR R-166, Dec. 1963, NASA.

[3]Heard, W. L., Jr. and Bohon, H. L., "Natural Vibration and Flutter of Elastically Supported Corrugation-Stiffened Panels—Experiment and Theory," TN D-5986, Oct. 1970, NASA.

[4]Carden, H. D., Durling, B. J., and Walton, W. C., Jr., "Space Shuttle TPS Panel Vibration Studies," TM X-2274, Vol. III, April 1971, NASA.

[5]Lemley, C. E., "Design Criteria for the Prediction and Prevention of Panel Flutter," AFFDL-TR-67-140, Vol. I, Aug. 1968, Air Force Flight Dynamics Lab., Wright-Patterson Air Force Base, Ohio.

[6]Erickson, L. L., "Supersonic Flutter of Flat Rectangular Orthotropic Panels Elastically Restrained Against Edge Rotation," TN D-3500, Aug. 1966, NASA.